Kerbala Journal of Pharmaceutical Sciences

ISSN: 2221-7207(Print) / **ISSN**: 3006-7189 (Online)

Antibacterial Effects of HA-Coated Cdsnps and Associated Changes in Stress-Responsive Efflux Gene Expression in MDR *Klebsiella Pneumoniae*

Noor Jasim Mohammed[1], Gerben J. Zylstra[2] and Thamer Y. Mutter[1*]

[1]Department of Biology, College of Science, University of Anbar, Ramadi, Iraq.

[2]Department of Biochemistry and Microbiology, School of Environmental and Biological Sciences, Rutgers University, New Brunswick, NJ, USA

*** Corresponding Author**

Thamer Y. Mutter: mthamir78@uoanbar.edu.iq

Received: 01/10/2025
Accepted: 08/11/2025
Published: 30/06/2026

Keywords: Cadmium nanoparticles, efflux pump, Gene expression, hyaluronic acid, *Klebsiella pneumoniae*.

DOI:10.62472/kjps.v17.i28.11-28

Abstract

Klebsiella pneumoniae is a global healthcare concern due to its robust efflux systems and ability to form biofilm, especially MDR strains. Our aim was to study the impact of hyaluronic acid-coated cadmium sulfide nanoparticles (CdSNPs-HA) on the expression of bacterial stress-responsive efflux genes. Green method utilizing *Raphanus sativus* root was used to synthesize the nanoparticles at an elevated temperature. Well diffusion methods were used to assess the minimal inhibitory concentration (MIC), and biofilm formation assays were determined using the 96-microtiter plate. Gene redundancy was identified using PCR, while gene expression was assessed using quantitative PCR (qPCR). The study's results of SEM and TEM showed a successful HA coating with uniform and stable core-shell rod-like nanostructures. Fifty clinical *Klebsiella pneumoniae* isolates showed resistance to piperacillin-tazobactam (100%), cefepime (76%), and ceftriaxone (72%). Eighty-six percent of the isolates demonstrated the ability to produce biofilm. PCR results indicated 100% presence of *acrB* and *oqxB* efflux pump genes. Antibacterial activity of coated nanoparticles showed enhanced activity compared to uncoated CdSNPs. The MIC of CdSNps-HA was 3.12 mg/mL, compared to 12.5 mg/mL, and a larger inhibition zone was observed (16 mm vs. 13 mm), respectively. RT-qPCR analysis demonstrated more than 6-fold upregulation of *acrB* and 1.2-fold upregulation of *oqxB* upon exposure to CdSNPs-HA, compared with downregulation of uncoated nanoparticles. This pattern of regulation reflects a stress-induced response to nanoparticle exposure rather than direct inhibition of efflux. This highlights the complex adaptation of bacteria and suggests that HA-coating influences resistance pathways in a gene-specific manner.

التأثير المضاد للبكتريا لجسيمات CdSNPs المغلفه بحامض الهيالورونيك والتغيرات المرتبطه في التعبير الجيني لجينات الدفق نتيجة الاجهاد في *Klebsiella pneumoniae* متعددة المقاومة للأدوية

نور جاسم محمد، كربن زيلسترا، ثامر يوسف مطر

الخلاصة

تُعدّ *Klebsiella pneumoniae* المقاومة المتعدّدة للأدوية تهديدًا سريريًا كبيرًا، ويعود ذلك لوجود مضخات الدفق (efflux) وتكوين الأغشية الحيوية. في هذه الدراسة، تمّ دراسة تأثير الجسيمات النانوية من كبريتيد الكادميوم المغلّفة بحمض الهيالورونيك (CdSNPs-HA)، والمحضّرة بالطريقة الخضراء باستخدام جذور الفجل *Raphanus sativus* عند درجة حرارة مرتفعة، في تعبير جينات مضخّات الدفق لدى عزلات سريرية من *K. pneumoniae* المتعدّدة المقاومة. جرى توصيف الجسيمات باستخدام حيود الأشعّة السينية (XRD) وطيف تحت الحمراء (FT-IR) والمجهر الإلكتروني الماسح (SEM) والنافذ (TEM). وقُيّم النشاط المضاد للبكتيريا بطريقة الانتشار على الاقراص، فيما حُدِّد MIC وتكوين الغشاء الحيوي باستخدام الصفائح البلاستيكية 96 حفرة. تم الكشف عن تردد الجينات بتقنية PCR، بينما قيس التعبير الجيني بتقنية RT-qPCR. أكّدت صور SEM وTEM نجاح التغليف بحمض الهيالورونيك وتشكّل جسيمات نانوية متجانسة ومستقرة بنواة-غلاف (core–shell) مع تجمّع أقل. شملت الدراسة خمسين عزلة سريرية جرى توصيف مقاومتها وقابليتها لتكوين الغشاء الحيوي؛ إذ أظهرت جميع العزلات مقاومة piperacillin-tazobactam (100%)، ونِسَب مقاومة مرتفعة cefepime(76%) و ceftriaxone (72%)، فيما أظهرت 86% منها قدرة على تكوين الغشاء الحيوي. كشف PCR وجود جيني acrB وoqxB في 100% من العزلات. أظهرت CdSNPs-HA نشاطًا مضادًا للبكتيريا أعلى من الجسيمات غير المغلّفة، مع MIC بلغ 3.12 mg/mL مقابل 12.5 mg/mL، وقطر منطقة تثبيط أكبر (16 mm مقابل 13 mm). أظهر تحليل RT-qPCR ارتفاعًا في تعبير acrB بأكثر من ستة أضعاف وارتفاعًا قدره 1.2 ضعف في oqxB بعد التعرّض لـ CdSNPs-HA، في حين أدّت الجسيمات غير المغلّفة إلى خفض ملحوظ في تعبير كلا الجينين (<0.01). تشير هذه الأنماط إلى استجابة مرتبطه بالإجهاد للتعرّض للجسيمات المغلّفة، وليس بسبب الكبح المباشر لمضخّات الدفق. ورغم أنّها ليست تأثيرًا كابحًا كلاسيكيًا للـ efflux، فإن تبدّل نمط التعبير يبرز تكيفًا جرثوميًا معقّدًا ويشير إلى أنّ تغليف الهيالورونك يؤثّر في مسارات المقاومة بأسلوب نوعي خاص بكل جين.

1. Introduction

The control of infectious diseases is becoming increasingly challenging because the rise in antibiotic resistance (Guo et al., 2020). The increase in bacterial infections and their spread is a common cause of antibiotic treatment failure in hospitals (Fils et al., 2021; Jassim and Hassan, 2023). More than 70% of bacteria causing hospital infections are found to be resistant to at least one of the antibiotics used for treatment; they can only be treated with experimental and potentially toxic drugs (Regassa et al., 2024). Several infections worldwide have been identified due to *K. pneumoniae*. It is classified as one of the ESKAPE pathogens, known for its ability to resist several antibiotics (Busi and Prasad, 2024). 60-80% of bacterial infections were associated with microbial biofilm formation, which is one of the main factors that increase the resistance to both antibiotics and host immune defenses (Sharma et al., 2023). Biofilms consist of populations of bacteria enveloped in a protective extracellular matrix, which enhances the resistance of *Klebsiella pneumoniae* to antimicrobial agents and various environmental stresses, thereby complicating the treatment of infections (Elashkar et al., 2025). There are several antibiotic resistance mechanisms, including the inactivation or alteration of antibiotics, modification of the targets, changes in metabolic pathways, and enhanced efflux systems. Large amounts of antibiotics and other toxic materials can be pumped out of bacterial cells using membrane permeability mediated by efflux genes (Mohanty et al., 2021; Huang et al., 2022). Their role in depleting different substrates is to maintain internal homeostasis, a major factor in bacterial survival (Gaurav et al., 2023). *acrAB, oqxAB,* and *kexD* are commonly associated with antibiotic resistance (Karami-Zarandi et al., 2023). Innovative strategies, such as nanoparticle synthesis, have been widely employed to develop various antibacterial agents and counteract the ongoing emergence of antibiotic resistance. Nanotechnology is offering high advantages in modulating efflux pumps and membrane permeability barriers (Hetta et al., 2023). Nanoparticles have been explored as an alternative approach to decrease the resistance mechanism, especially in multidrug resistance. They interact with bacterial DNA and cell walls, disrupt biofilm formation, and induce the generation of reactive oxygen species (ROS), making them potential candidates for treating bacterial infections (Ahmed et al., 2021). Nanoscale dimensions, large surface area, and customizable surface chemistry make nanoparticles a target of interest for use in biomedical applications (Hamid et al., 2024; Ali et al., 2024; Al-Darwesh et al., 2025). Nanoparticles can operate through various modes of action, thereby enhancing their effectiveness against multidrug-resistant (MDR) bacterial strains (Adeniji et al., 2022). Cadmium sulfide is an inorganic compound with unique optical and electronic properties. It was utilized in nanoparticle synthesis used in biomedical applications, particularly in the form of cadmium-based quantum dots (Rather et al., 2022; Ebrahim et al., 2023; Badry et al., 2024). Despite the toxicity of cadmium, it has been used as a nanocomposite of different combinations resulted in enhanced antibacterial and antibiofilm activity due to the generation of reactive oxygen species and the release of Cd^{+2} ions that affect the membrane permeability (Adeli-Sardou et al., 2022; Abbas et al., 2023; Kaliyaperumal et al., 2025). However, its toxicity is still a major concern among researchers (Dabhane et al., 2021). To mitigate the toxic effects, coating or nanocapsulating with organic compounds has been recently used to reduce the toxicity of metals (Zayerzadeh and Koohi, 2024; Dubey et al., 2025). Building upon our previous findings, where cadmium sulfide nanoparticles exhibited promising antimicrobial properties (Mohammed et al., 2025), this study investigates whether a strategic hyaluronic acid coating, combined with green synthesis at elevated temperatures, can improve nanoparticle stability, bioavailability, and ultimately modulate efflux pump gene expression in K. pneumoniae. Under elevated temperatures, synthesis methods have shown improvements in the crystallinity and size control of synthesized

nanoparticles (Spitzmuller et al., 2023). These modifications helped disrupt bacterial cells and affect efflux gene expression, contributing to reduced antimicrobial resistance.

2. Materials and Methods

2.1. Collection of Clinical Samples

A total of 50 clinical specimens of *Klebsiella pneumoniae* were collected from patients with various conditions, including urinary tract infections, respiratory sputum, and blood infections, at AL-Ramadi Teaching Hospital. The samples were cultured on MacConkey agar and incubated at 37°C for 24 hours. Then, isolates grown on MacConkey agar were characterized using biochemical tests and confirmed by the VITEK 2 system. Ethical approval was obtained from the University of Anbar Ethics Committee (Ref. 239, 24 February 2024), in accordance with national ethical standards, prior to sample collection.

2.2. Antibiotic Susceptibility Assessment

Antimicrobial susceptibility testing was performed with the Kirby-Bauer disk diffusion method, as per the recommendations of the Clinical and Laboratory Standards Institute (Lewis, 2024). Muller-Hinton agar was used as the culture medium. Gentamicin (GM, 10 µg), Cefepime (FEP, 30 µg), Ceftriaxone (CRO, 30 µg), Piperacillin-tazobactam (PIT, 100/10 µg), Tetracycline (TE, 15 µg), Imipenem (IPM, 10 µg), Levofloxacin (LEV, 5 µg), and Ciprofloxacin (CIP, 5 µg) were used to assess the resistance profile of *Klebsiella* isolates.

2.3. Biofilm Formation Assay

The ability of *K. pneumoniae* to form biofilm was assessed using the crystal violet method in a 96-well microplate, with minor modifications as described in (Khaleel et al., 2025a). Briefly, *K. pneumoniae* was isolated after being grown in nutrient broth at 37°C with shaking at 150 rpm for overnight incubation. A dilution of 200µL (1.5×10^8 CFU/mL) was pipetted into each well of the plate. Then, the plates were incubated at 37 °C for 48 hours. After the incubation period, the wells were washed with ddH2O three times to remove unbound cells. All wells were treated with 200µL of 1% (w/v) crystal violet suspension and incubated for another 30 minutes. The dye was spilled out of the plate by inverting the plate, and another washing cycle was done using ddH2O to remove any excess or unbound dye. Ethanol (95%) was then added to solubilize the dye, with 200 µL pipetted into each well. Optical density was measured using a spectrophotometer at an OD of 570 nm. The biofilm assay was performed in triplicate, and the mean values were calculated to determine the biofilm formation according to the following measurements:

$OD \leq ODc$	Non producer
$ODc < OD \leq 2 \times ODc$	Weak producer
$2 \times ODc < OD \leq 4 \times ODc$	Moderate producer
$OD > 4 \times ODc$	Strong producer

2.4. Efflux Pump Genes

To determine the distribution of the efflux pump genes among the characterized isolates, polymerase chain reaction (PCR) was conducted using 2x Easy Taq® PCR Super Mix (Promega, USA). Efflux pumps genes were amplified using the primers OqxB-F: GCTGTTCGGTCTGTTCCTGA and OqxB-R: TTGCAGATGGTTCTCAGCGT for *oqxB* amplification; AcrB-F: TATCGGCTACGACTGGACC and AcrB-R:

GCCCTTTGCCCTCTTTCT for *acrB* amplification (Xu et al., 2019). PCR reaction of 20 µL was performed by mixing 10µL of 2X Master Mix, 1µL of forward primer (0.4 µM), 1µL of reverse primer (0.4 µM), 1µL of genomic DNA (20 ng), and ddH_2O to bring the final volume to 20 µL. The subsequent conditions were employed in a Bio-Rad T100 Thermal Cycler (UK): primary denaturation (1 cycle) for 5 minutes at 95°C; denaturation for 30 seconds at 95°C, annealing for 40 seconds at 55°C, extension for 40 seconds at 72°C (25 cycle), and a final extension for 10 minutes at 72°C (1 cycle). The reaction results were evaluated using electrophoresis with 1.2% agarose and visualized under Bio-Rad gel electrophoresis documentation system.

2.5. Green Synthesis of CdSNPs and CdSNPs-HA

Fig.1. illustrates the route synthesis of cadmium sulfide nanoparticles (CdSNPs). Fresh root of *Raphanus sativus* was obtained from the AlRamadi local market. After being cleaned with double-distilled water, the roots were ground using a mortar and pestle. 5 g was mixed with 50 mL of ddH2O and left on a magnetic stirrer hot plate for 30 minutes at 60°C. *R. sativus* extract was separated using a centrifuge after being filtered through a 47 mm Whatman filter paper. Then, the resulting extract was stored at 4°C until further use (Al Awadh et al., 2022). Cadmium sulfide nanoparticles (CdS NPs) were prepared following the procedure indicated in (Dalei, 2014) with modifications. 20 mL of the extract was added dropwise to 80 mL (0.1 M) of cadmium nitrate solution ($Cd(NO_3)_2$). Then, 80 ml of Na2S (0.1 M) was gradually added to the mixture and left on a magnetic stirrer at 95°C for 1 hour or until the color changed to yellow-orange, which indicates the formation of Cadmium sulfide nanoparticles (Fig.1). CdS Np was washed with deionized water three times, centrifuged at 10000 rpm for 15 minutes to remove unreacted materials, and then dried at 50 °C. A hyaluronic acid solution (0.1%) was prepared by dissolving 0.18 g of hyaluronic acid powder (molecular weight = 8 kDa) in 180 mL of distilled water. Then, 100 mL of the prepared solution was added dropwise to 100 mL of CdS nanoparticles and maintained on a magnetic stirrer at 60 °C for 2 hours. Afterward, the sample was centrifuged for 15 minutes at 10,000 rpm, rinsed three times with distilled water, and dried in an oven set at 50 °C.

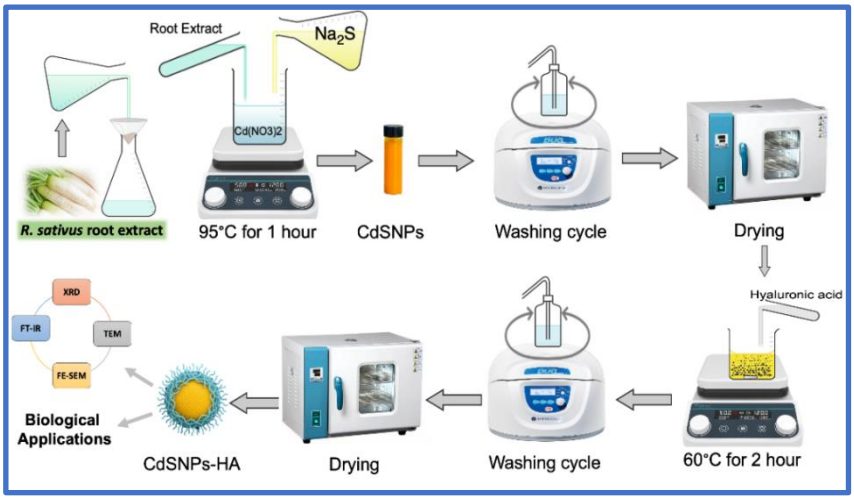

Figure1: Schematic illustration of the green synthesis and hyaluronic acid functionalization of cadmium sulfide nanoparticles (CdSNPs). Root extract of Raphanus sativus was used as a bioreducing and stabilizing agent for the synthesis of CdSNPs through the reaction of cadmium nitrate [$Cd(NO_3)_2$] and sodium sulfide (Na_2S) at 95°C for 1 h. The synthesized CdSNPs were purified by repeated washing and drying. Subsequently, the nanoparticles were coated with hyaluronic acid (HA) by incubation at 60°C for 2 h, followed by washing and drying to obtain HA-functionalized CdSNPs (CdSNPs-HA). The resulting nanocomposite was characterized using XRD, FT-IR, TEM, and FE-SEM and evaluated for its biological applications.

2.6. Physicochemical Characterization of Synthesized Nanoparticles

Structural and morphological characterization were used to analyze the synthesized cadmium sulfide nanoparticles (CdSNPs). Fourier Transform Infrared Spectroscopy (FTIR) (Bruker ALPHA II spectrophotometer, Germany) was used to identify the functional groups in synthesized nanoparticles. 5 µL of liquid samples and oven-dried CdSNP powders were pressed against the crystal surface. Spectra were recorded across the 450- 4000 cm^{-1} range, with 32 scans at a resolution of 4 cm^{-1}. Crystalline structure and phase identification were analyzed using X-ray diffraction (Malvern Panalytical Empyrean diffractometer, UK), operated at 40 kV and 30 mA with CuKα radiation (λ = 1.540598 Å). Samples were scanned over a 2θ range of 10°-70°. Crystalline sizes were calculated by the Scherrer equation. Surface morphology and topographical details of the nanoparticles were examined via Scanning Electron Microscopy (SEM) using Inspect™ F50 system (FEI, Netherlands). Further insight into nanoparticle morphology, size distribution, and dispersion was obtained using Transmission Electron Microscopy (TEM) with a Zeiss Leo 912 AB microscope (Germany) at 80 kV. TEM measurements was used and over 100 individual particles were taken from each sample to determine average particle size.

2.7. MIC Assay

Minimum inhibitory concentration (MIC) was performed to determine the lowest concentration of the synthesized nanoparticles that prevents observable bacterial growth. The minimum inhibitory concentration of the CdSNPs and CdSNPs-HA against *K. pneumoniae* isolates was determined using the broth dilution method, as described by the Clinical and Laboratory Standards Institute (CLSI). The procedure indicated in (Khaleel et al., 2025b) was followed with minor modifications. Briefly, 100 µL of Muller-Hinton broth was added to the wells of a 96-well plate. A repeated two-fold dilution of 100 µL of CdSNPs and CdSNPs-HA was conducted. Subsequently, 10µL of freshly cultured bacteria (OD_{600}=0.05) was added into each well. Wells lacking any antibiotic agent served as the positive control, and the medium without any bacterial inoculum served as the negative control. The plates were incubated at 37 °C for 24 hours. After the incubation, 20 µL of a resazurin dye solution (0.01 g/100 mL) was introduced to each well. The plates were subsequently re-incubated at 37 ℃ for an additional 2 hours. The color transition from blue (oxidized state) to pink (reduced state) indicated bacterial growth. The MIC was identified as the minimum dose of CdSNPs and CdSNPs-HA that inhibited color change.

2.8.Antimicrobial Activity

Antimicrobial susceptibility testing was conducted using the standard well diffusion method as described in (Lewis, 2024). Bacterial cultures (*K. pneumoniae*) were first cultivated in nutrient broth for 24 hours at 37 ℃. Then, Bacterial growth (OD_{600}=0.5) was inoculated on Mueller-Hinton agar plates (HI Media) using a sterile cotton swab. Wells of 5 mm diameter were created in the agar utilizing a sterile cork borer. Each well was filled with 50 µL of sonicated CdSNPs (10 mg/mL) and CdSNPs-HA (10 mg/mL), HA (10 mg/mL), plant extract (PE) (10 mg/mL), and $Cd(NO_3)_2$ (10 mg/mL). The plates were incubated at 37°C for 24 hours. Following incubation, the sizes of the inhibitory zones were measured in millimeters and documented.

2.9.Expression of Efflux Pump Genes

The effect of the synthesized nanoparticles on the expression of *oqxB* and *acrB* genes in *Klebsiella pneumoniae* was determined using real-time PCR (RT-PCR) using the primers (designed in this study) oqxB-RF: GATATCACGCAGGGTGATCTT and oqxB-RR: TGAACGTTCGACGAGTGCGA; acrB-RF: TATTGCGTTCTTCGCCGACA and acrB-RR: GCTGATTGTCGTCTTCCTGT. *rpoD* was used as the housekeeping gene using the primers rpoD-F: AGATGGTTGAAGCGAACCTG and rpoD-R: CGAACTTATCGACCGCTTTC (Khaleel et al., 2024). Bacterial RNA was extracted and purified using the

TRIzol kit (Transgene, China). RNA was converted to cDNA using an Easy Script® One-step removal and cDNA synthesis super-Mix kit (Transgene, China) following the manufacturer's instructions. qPCR was done using Perfect Start® Green qPCR Super Mix (+Universal Passive Reference Dye). Reactions were prepared in a final volume of 20 µL containing 10 µL 2X master mix, 1µL forward primer (0.2 ng), 1 µL reverse primer (0.2 ng), 3 µL cDNA (5 ng), and 5 µL of dH2O. RT-qPCR was carried out in an RT-qPCR machine from Bioer, China, and the RNA concentrations were quantified using a Nanodrop OneC from thermosfisher. PCR results were analyzed using the relative quantification ($\mathbf{2^{-\Delta\Delta CT}}$).

2.10. Statistical Analyses

Graphs and statistical analyses were performed using GraphPad Prism version 8. Data are presented as mean ± standard deviation (SD). Comparisons between groups were assessed using Dunnett's multiple comparison test.

3. Results and Discussion

3.1. Bacterial Identification: Resistance Profiling and Biofilm Assessment

The 50 *Klebsiella pneumoniae* isolates were obtained from clinical specimens, including urine, blood, and sputum. Fig.2. shows the results of the phenotypic and biochemical tests. The isolate showed a typical profile of *Klebsiella pneumoniae* characterized by lactose fermentation on MacConkey agar, positive citrate utilization, urease activity, and positive Voges-Proskauer test. These characterizations were further confirmed using the VITEK. The results indicated 20 (40%) isolates with positive mucoid string formation characteristics of hypermucoviscous.

Antibiotic susceptibility testing indicated a high prevalence of multidrug-resistant isolates. All isolates showed complete resistance (100%) to piperacillin-tazobactam, with similarly high resistance rates observed for cefepime (76%) and ceftriaxone (72%), followed by gentamicin (40%), levofloxacin (30%), tetracycline (24%), and ciprofloxacin (22%), as shown in Table1. Interestingly, imipenem retained substantial activity with 80% of isolates sensitive, recording its continued relevance as a last-line therapeutic agent. However, this resistance percentage represents a higher rate compared to previous studies performed in the same region, where Al-Fahdawi et al. (2023) reported 93.88% sensitivity and Khaleel et al (2025a) found 100% sensitivity to imipenem.

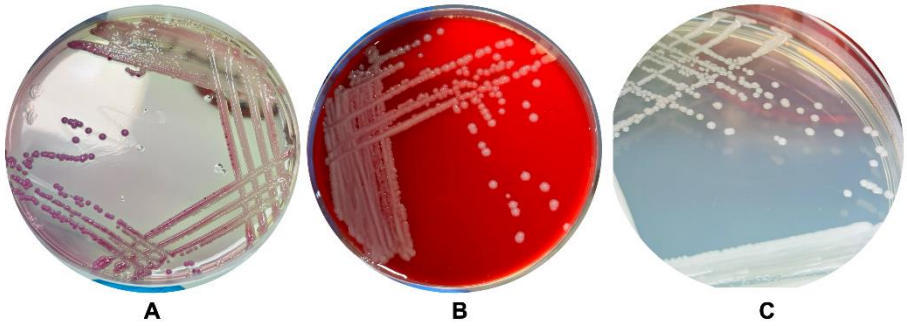

Figure2: *Klebsiella pneumoniae* grown on (A) MacConkey agar; (B) Blood agar; (C) Nutrient agar.

Table1: Antimicrobial-Resistant Profile of *Klebsiella* Isolates

Class	Antibiotic	Concentration (µg)	Resistance Profile % (n=50)
Aminoglycosides	Gentamicin	10	40 (20)
Cephalosporins	Cefepime	30	76 (38)
	Ceftriaxone	30	72 (36)
β-lactam	Piperacillin - tazobactam	100/10	100 (50)
Tetracyclines	Tetracycline	30	24 (12)
Carbapenem	Imipenem	10	10 (5)
Fluoroquinolone	Levofloxacin	5	30 (15)
	Ciprofloxacin	5	22 (11)

Biofilm formation was detected in 43 (86%) isolates, with 32.5% weak producers, 46.5% moderate producers, and 21% strong biofilm producers, as shown in Fig. 3. Biofilm production may contribute to the high resistance profile, as it prevents antibiotic penetration and facilitates persistent colonization (Sharma et al., 2023). Moreover, the positive string test observed in several isolates may indicate the presence of hypermucoviscous phenotypes, which are associated with increased virulence and invasive disease Al-Fahdawi et al., 2023). Our study isolates showed higher rate of biofilm formation and antibiotic resistance, indicating a correlation between the two profiles (Ali et al., 2019; Obaid and Hasson, 2021; Alansary and Al-Saryi, 2022) . The ability of *K. pneumoniae* to resist different antibiotics and form biofilm elevates the risk associated with its infection and elevates the urgent need looking for new therapeutic agents.

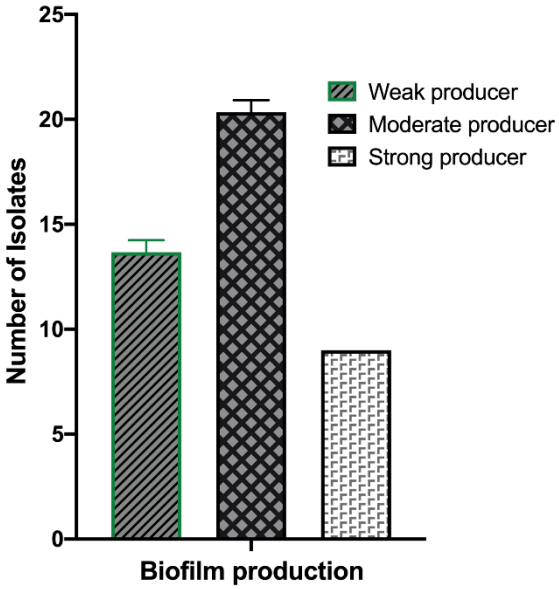

Figure3: Number of *K. pneumoniae* isolates able to form biofilm. 32.5% weak producers, 46.5% moderate producers, 21% strong producers.

3.2. Redundancy of Efflux Pump Genes

oqxB and *acrB* were detected using PCR as mentioned in the methods. Both genes were highly redundant (100%) in all 50 *K. pneumoniae* isolates, as illustrated in Fig. 4. This distribution strongly correlates with the extensive multidrug-resistant profile discussed above. The two genes are well documented as mediators of resistance to

beta-lactams, fluoroquinolones, aminoglycosides, and tetracyclines by pumping these antibiotics out of the bacterial cell, decreasing their concentrations and promoting MDR phenotypes (Li et al., 2019). Efflux pump genes contribute to biofilm formation by enhancing quorum-sensing proteins and adhesions, while also increasing the export of extracellular substances necessary for biofilm development. This creates a feedback loop where efflux activity and biofilm production mutually reinforce one another (Hajiagha and Kafil, 2023; Ren et al., 2024).

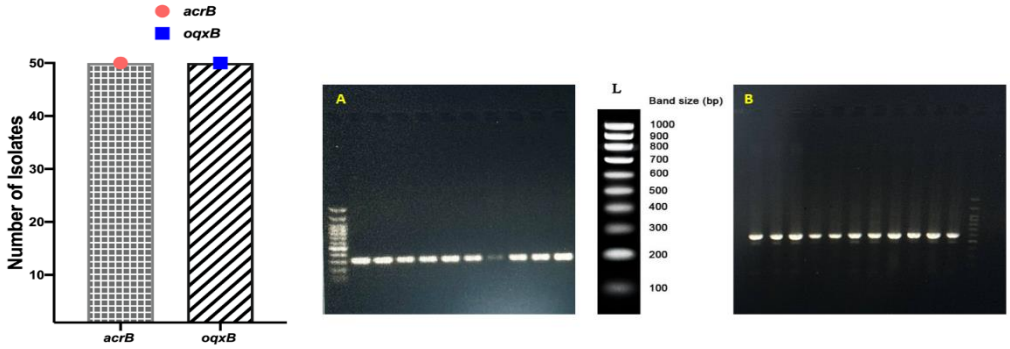

Figure4: Left: number of efflux pump genes among *K. pneumoniae* isolates; right: Gel electrophoresis of the PCR products using 1.2% agarose: A) *AcrBp*, B) *OqxBp*

3.3. Structural and Chemical Characterization of Nanoparticles

The structural and chemical characteristics of CdSNPs synthesized via a green route using *Raphanus sativus* root extract were thoroughly investigated using XRD and FTIR spectroscopy. The XRD profile of the synthesized material exhibited a series of intense and well-resolved diffraction peaks positioned at approximately 2θ = 24.8°, 26.5°, 28.2°, 36.7°, 43.8°, 47.8°, and 51.9°, corresponding to the (100), (002), (101), (102), (110), (103), and (112) planes, respectively (Fig.5). These reflections correspond to the standard hexagonal wurtzite structure of CdS, as indexed in JCPDS card number 96-900-8863 (Aljarrah and Aljobory, 2017). The absence of additional reflections, such as those associated with the cubic polymorph or other impurity phases, indicates the successful formation of a single-phase hexagonal structure with high purity (Yaaqoub and Abbas, 2023). The sharpness and intensity of the peaks suggest a high degree of crystallinity, which is typically attributed to the controlled nucleation and growth processes facilitated by phytochemical agents in the plant extract under elevated temperature Fig. 6 shows the spectrum of the crude extract that indicates broad absorption bands near 3450 cm^{-1}, matching the O-H stretching from hydroxyl groups, as well as bands at 2920 and 2850 cm^{-1} matching the asymmetric and symmetric C-H stretching vibrations. Additional peaks of 1380-1120 cm^{-1} could be assigned to C-O stretching and O-H bending, associated with alcohols, carboxylic acids, and other plant-derived phenolics. FTIR spectrum showed a shift and reduction in the band intensity, referring to their involvement in the reduction of cadmium ions and stabilization of the resulting nanoparticles. The bands appeared at ranges of 650-550 cm^{-1}, which might be a characteristic of Cd-S bond vibrations, confirming the formation of the CdS nanoparticles. A band observed near 1100 cm^{-1} may be attributed to C-N stretching vibrations, indicative of amine compounds in the extract that serves as a capping agent. These results clearly reflect the participation of phytoconstituents in the nanoparticle synthesis process. Hydroxyl, carboxyl, and amine functional groups are most likely to be coordinated with cadmium ions during the reduction step and subsequently bind to the nanoparticle surface, thereby preventing agglomeration

and promoting colloidal stability (Pedroso-Santana and Fleitas-Salazar, 2023). This dual functionality highlights the efficiency of *Raphanus sativus* root extract in facilitating the environmentally benign synthesis of nanoparticles.

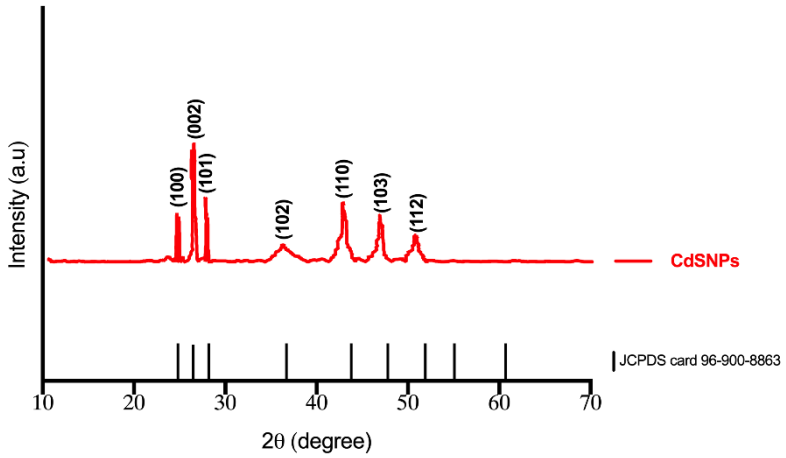

Figure5: XRD Analysis of The Synthesized CdSNPs in Accordance with The Standard Cadmium Standard Cassette (JCPDS card no. 96-900-8863)

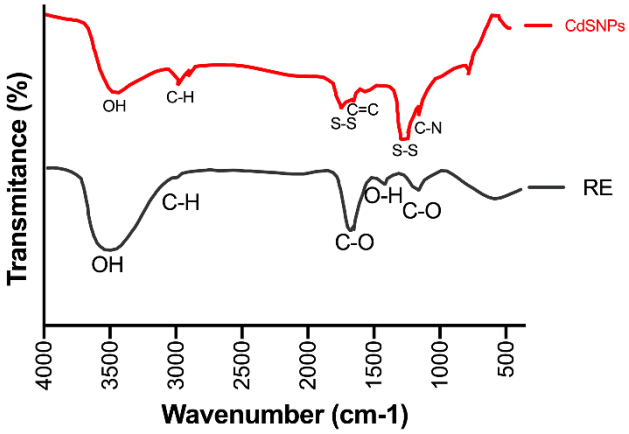

Figure6: FTIR Shows the Functional Groups of The Synthesized Nanoparticles

3.4. SEM Characterizations

Fig.7. shows the surface morphology of CdS-NPs and CdSNPs-HA using SEM analysis. The results indicate differences in the surface and the structural uniformity of the two types of nanoparticles. Fig.7a and 7c indicate irregular particle with variations in the sizes and morphology in uncoated nanoparticles. Random distributions were noticed with agglomeration across the surface. A quantitative analysis of 81 particles was conducted using ImageJ, that showed a wide range of sizes, 36.4 to 136.7 nm with a mean size of 59.5 nm. The coated CdSNPs displayed a smoother and more regular surface morphology (Fig.s 7b and 7d). The sharpness and angular features of the uncoated nanoparticles disappeared and more homogeneous surface structure was identified. This transformation an indicative of the successful coating by HA. HA acts as a steric barrier and prevents particle-particle fusion, promoting high dispersion (Kim et al., 2023; Li et al., 2024). The particle size ranged from 31.4 to 93 nm with an average size of 49.4 nm.

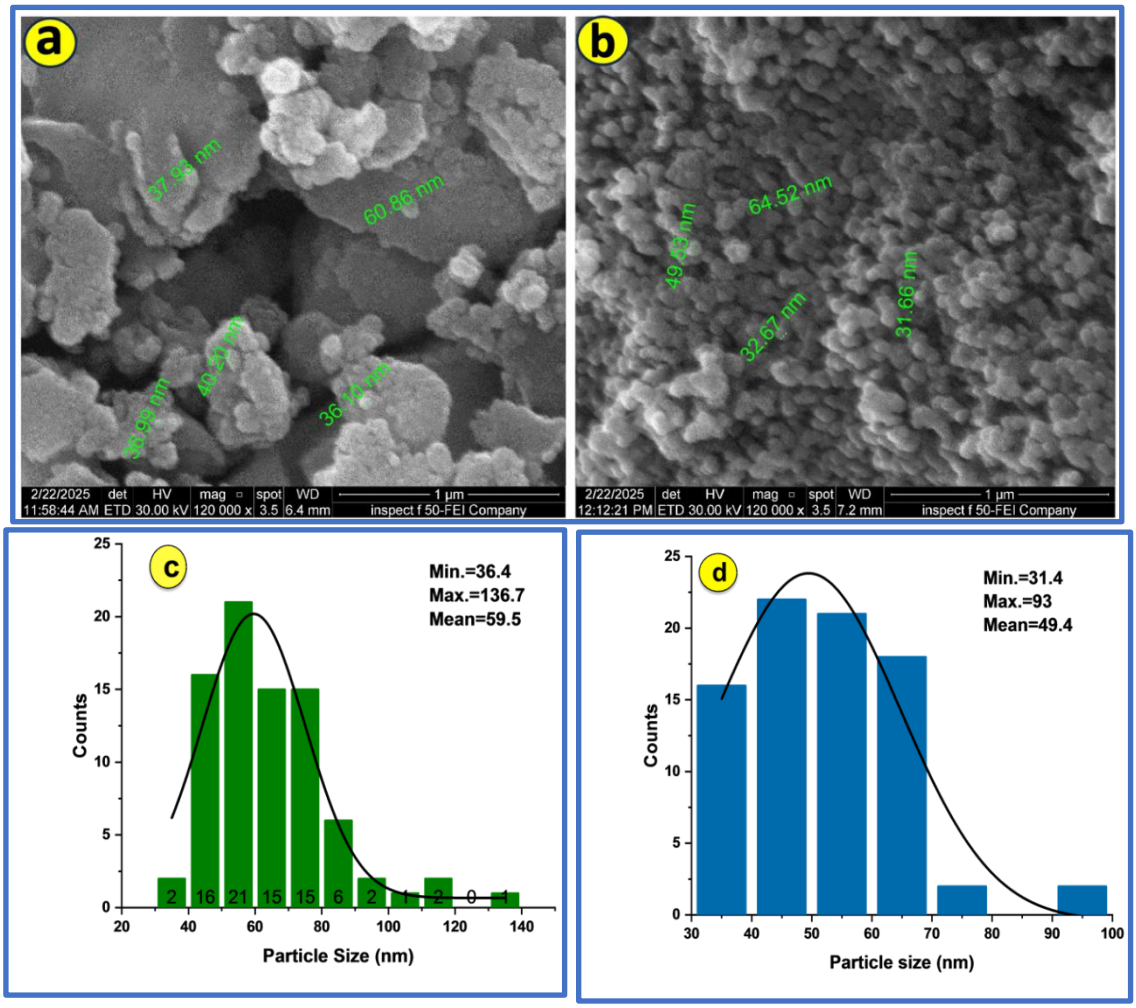

Figure7: Scanning Electron Microscope of The Synthesized Nanoparticles at 1µm: (a) CdSNPs, (b) CdSNPs-HA, (c) particle distribution of CdSNPs with a mean of 59.5 nm, (d) particle distribution of CdSNPs-HA with a mean of 49.4 nm

3.5.Structure Evaluation

The CdSNPs appeared as clusters and aggregated with different shapes, exhibiting irregular morphology when tested using TEM (Fig. 8a). The uncoated nanoparticles appeared with nanorod- structures, suggesting anisotropic growth matching the XRD results that showed a direction of the wurtzite lattice (001), which is a known preferential axis for cadmium nanorod formation. The temperature used in the synthesis played a major role in the production of rod-like nanoparticles (Liu et al., 2017; Kushwaha and Chauhan, 2021). Anisotropic growth can be formed from uneven growth in different directions, which can be enhanced when leftover precursor molecules attach selectively to certain crystal surfaces during nanoparticle synthesis. This led to oriented attachment, in which small nanocrystals arrange and join to form the nanorods (Liu et al., 2023). Coated cadmium sulfide nanoparticles exhibited a unique morphological shift, featuring a rod-like CdS core encapsulated by an outer layer, which formed a well-defined core-shell structure (Fig.7b). The outer layer is a confirmation of the HA that envelopes and extends uniformly around the crystalline core with a thickness of 8-12 nm on each side. The increased particle diameter confirms the formation of the coating with HA. These matches with a previous report describing similar morphological effects in HA-functionalized nanomaterials (Yahyaei, 2016). Electrostatic

interactions between the anionic carboxyl groups of HA and the positive charge of Cd ions are one of the mechanisms known in HA coating, in addition to hydrogen bonding and chelation effects may also play a role in the coating process (Liu et al., 2022; Le and Le Cerf, 2022). This coating by HA is not only reduce the particle aggregations and stability, but mitigates the intrinsic cytotoxicity of cadmium nanoparticles as a result of the formation of shell around the synthesized nanoparticles.

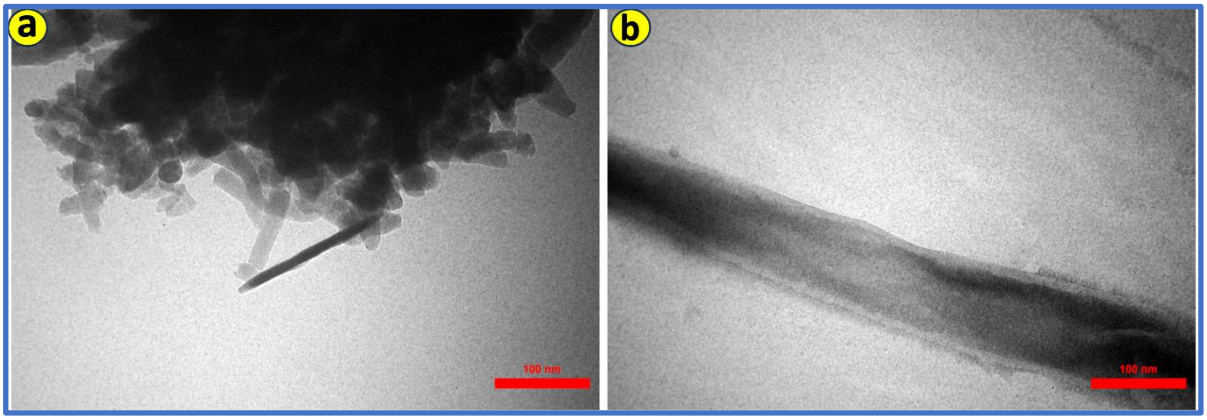

Figure8: TEM micrographs at 100 nm of (a) CdSNPs and (b) CdSNPs-HA indicating the shell envelop surrounding the CdS nanoparticles, thickness of 8-12 nm on each side.

3.6. MIC Value and Antibacterial Activity of CdSNPs and CdSNPs-HA

The antibacterial efficacy of cadmium sulfide nanoparticles (CdSNPs) and their hyaluronic acid-functionalized counterpart (CdSNPs-HA) was evaluated using agar well diffusion. The zone of inhibition assay, illustrated in Fig. 9, revealed a clear enhancement in antibacterial performance following HA coating. Specifically, the CdSNPs-HA nanocomposite produced a distinctly larger zone of inhibition, measuring 16 mm, compared to 13 mm observed with uncoated CdSNPs. No inhibition zones were observed when HA and plant extract (PE) used as antibacterial. This is consistent with their role as a coating and reducing agent. Surface modification using hyaluronic acid enhanced the antimicrobial activity of CdS nanoparticles.

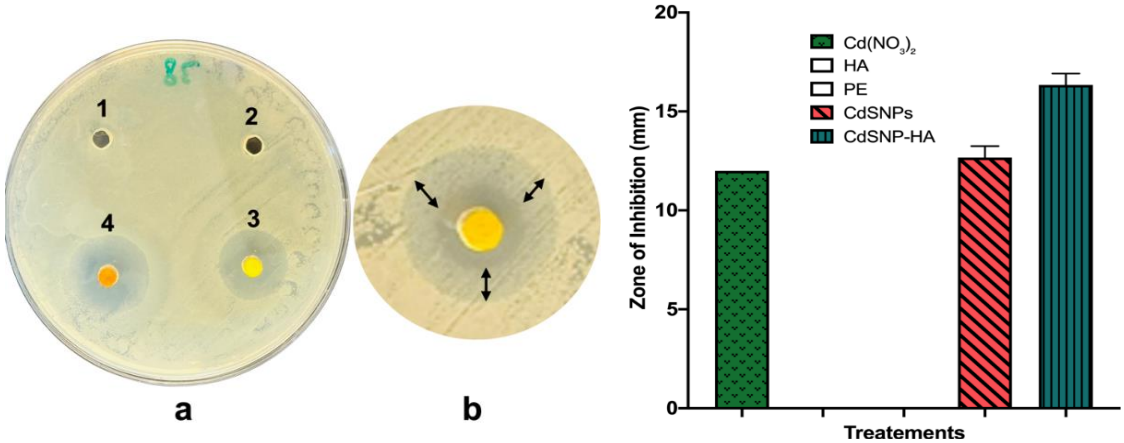

Figure9: (a) Petri dishes of antibacterial activity of (1) HA, (2) PE (plant extract), (3) CdSNPs, (4) CdSNPs-HA; (b) magnification of the inhibition zone indicating the overgrowth. The graph indicates the zone of inhibition in mm. Values are means from triplicate measurements, with error bars indicating ± SD.

The MIC results further confirmed the effectiveness of the synthesized nanoparticles. CdSNPs-HA had 3.12 mg/mL of MIC, which is lower than the MIC of 12.5 mg/mL recorded for uncoated CdSNPs. The reduction in expression fold highlights the critical role of using HA in nanoparticle efficiency. The superior activity of CdSNPs-HA is mostly attributed to multiple interrelated factors. Some of these factors enhance the colloidal stability and dispersion of the nanoparticles, preventing aggregation and providing a more uniform distribution in the bacterial environment. HA exhibits a biological affinity for cellular membranes, facilitating closer interaction and stronger adhesion between the CdS core and the bacterial surface (Alipoor et al., 2022; Kim et al., 2023). This may lead to increased membrane disruption, induction of oxidative stress, and interference with intracellular components. Bactericidal effect was most likely to occur to the bacteria, as indicated by the inhibition zone around CdSNPs-HA (well 4), while the over-growth noticed within the inhibition zone of uncoated CdSNPs (well 3) points toward a bacteriostatic mechanism. The HA coating plays a decisive role in maintaining a lethal interaction with bacterial cells over time, possibly by prolonging retention at the site of action (Zamboni et al., 2022; Curcio et al., 2022; Hovhannisyan et al., 2023; Bokatyi et al., 2024; El-Hamid et al., 2024; Raval and Bhattacharya, 2025). In general, these results demonstrate that HA functionalization significantly enhances the potential activity of CdS nanoparticles. The data strongly support the application of biopolymer-coated nanomaterials in the development of more efficient, targeted antibacterial agents. Further studies are warranted to explore the mechanism of action, stability in biological environments, and potential for resistance development of these compounds, thereby validating their clinical applicability.

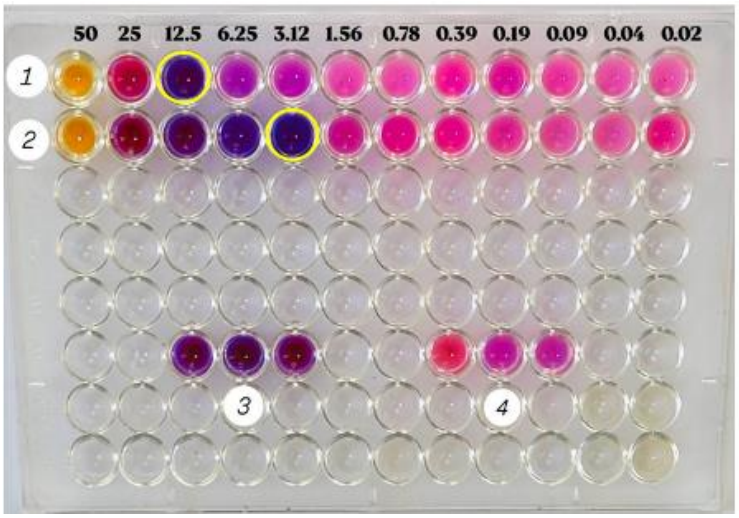

Figure10: MIC plate showing (1) CdSNPs, (2) CdSNPs, (3) negative control (only medium), (4) Positive control (medium + bacterial growth) against *K. pneumoniae*

3.7. Profile of *acrB* and *oqxB* Expression

The results in Fig.11 show the expression profile of the two efflux pump genes, *acrB* and *oqxB*, in response to the synthesized nanoparticle. The *acrB* encodes a key component of the acrAB-TolC efflux pump system responsible for pumping a wide range of materials, including antibiotics (Jang, 2023). Our results indicated an upregulation in acrB (>6-fold change) with CdSNPs-HA treatment. The HA coating may enhance stability and cellular interaction, leading to a stress response and activation of the efflux pump (Aibani et al., 2021). While the $Cd(NO_3)_2$ treatment resulted in a moderate upregulation (<3-fold change), which agrees with a previous study, indicating that heavy metal ions like Cd^{+2} can induce stress-mediated activation of those genes (Nag and Mehra, 2021).

Treatment with CdSNPs caused downregulation of acrB (<0.01-fold change), suggesting a high response to cellular toxicity. Similar patterns were observed with uncoated nanoparticles, leading to oxidative stress and DNA damage (Nasrin et al., 2019). The influence of HA and plant extract on gene expression was shown to have a slight downregulatory effect (<0.5-fold change). The phytochemical and HA nature are known for their membrane-protective properties in suppressing stress-gene expression (Ashraf et al., 2024). The *oqxB* gene belongs to the RND family and is an efflux pump system that is associated with exporting fluoroquinolones and detergents (Albarri et al., 2022). The *oqxB* expression showed unchanged in fold across most treatments with mild upregulation (1.2-fold change) seen with CdSNPs-HA treatment. This suggests limited activation. Moreover, this may indicate gene-specific regulatory response attributed to substrate affinity between the two gene systems (Bharatham et al., 2021). A significant suppression of *oqxB* expression was observed when bacteria were treated with CdSNPs and plant extract, less than a 0.02-fold change. This might suggest a complete shutdown of the transcriptional processes, probably due to an interference with the regulatory elements that regulate *oqxB* (Chan et al., 2022). In contrast, treatment with HA exhibited a similar pattern to that of the *acrB* gene, showing mild downregulation. This effect can be attributed to the stabilizing properties of HA in reducing the bacterial need to activate stress response genes. Similar trends in results showed that treatment with organic acids suppresses the level of mRNA required for capsular-associated genes in *K. pneumoniae* (Khaleel et al., 2024).

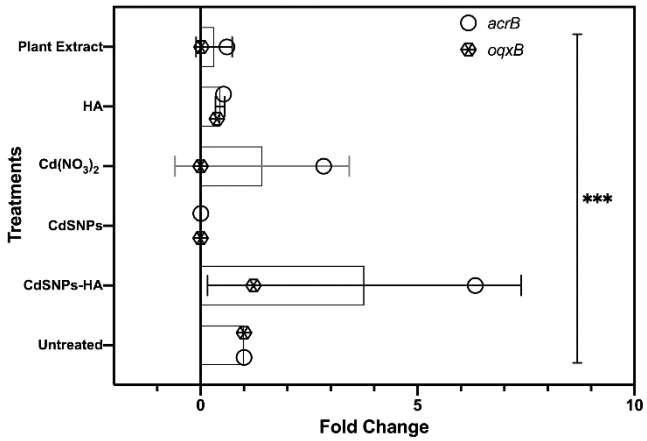

Figure11: Fold changes of gene expression (acrB and oqxB) after treatments with synthesized nanoparticles. Experiments performed in triplicate and data presented as mean ± SD (***=p<0.001)

Conclusions

The synthesized nanoparticles demonstrated improved stability and enhanced antibacterial activity. Efflux pumps regulation resulted in stress-induced response as a result of using CdsNPs-HA, which was clearly indicated by the upregulation of acrB. These results demonstrate that using HA can modify bacterial adaptation indirectly by inhibiting the efflux genes. This study strongly suggests the promising use of synthesized nanoparticles as antibacterial and anti-efflux agents after assessing their toxicity prior to biomedical use.

Author contribution

NMJ performed the experiments, investigation, analyzed the results, and wrote the original manuscript. GZ and TYM are supervising, analyzing, reviewing, and editing the manuscript.

Data availability

All data are present in this paper.

References

Abbas, B., Ul Ahmad, A., Shabbir, S., et al., 2023. Enhancing photocatalytic and antibacterial performance through compositional optimization of NiO-CdO heterogeneous nanocomposites. *Ceramics International.* 49(21), 33525–33536. DOI: 10.1016/j.ceramint.2023.07.250.

Adeli-Sardou, M., Shakibaie, M., Forootanfar, H., et al., 2022. Cytotoxicity and anti-biofilm activities of biogenic cadmium nanoparticles and cadmium nitrate: A preliminary study. *World Journal of Microbiology and Biotechnology.* 38(12), 246. DOI: 10.1007/s11274-022-03418-x.

Adeniji, O.O., Nontongana, N., Okoh, J.C., et al., 2022. The potential of antibiotics and nanomaterial combinations as therapeutic strategies in the management of multidrug-resistant infections: A review. *International Journal of Molecular Sciences.* 23(23). DOI: 10.3390/ijms232315038.

Ahmed, F.Y., Aly, U.F., El-Baky, A., et al., 2021. Effect of titanium dioxide nanoparticles on the expression of efflux pump and quorum-sensing genes in MDR *Pseudomonas aeruginosa* isolates. *Antibiotics.* 10(6). DOI: 10.3390/antibiotics10060625.

Aibani, N., Rai, R., Patel, P., et al., 2021. Chitosan nanoparticles at the biological interface: Implications for drug delivery. *Pharmaceutics.* 13(10), 1686. DOI: 10.3390/pharmaceutics13101686.

Al Awadh, A.A., Shet, A.R., Patil, L.R., et al., 2022. Sustainable synthesis and characterization of zinc oxide nanoparticles using *Raphanus sativus* extract and its biomedical applications. *Crystals.* 12(8), 1142. DOI: 10.3390/cryst12081142.

Al-Darwesh, M.Y., Hamid, L.L., Ibrahim, S.S., et al., 2025. Construction and characterization of 5,6-O-isopropylidene-L-ascorbic acid-loaded silver and manganese dioxide nanoparticles: Cytotoxicity study, antibacterial, and antioxidant activities. *Materials Chemistry and Physics.* 335. DOI: 10.1016/j.matchemphys.2025.130517.

Al-Fahdawi, A.M., Zylstra, G.J., Mutter, T.Y., 2023. Molecular and phenotypic detection of siderophore production by hypervirulent *Klebsiella pneumoniae*. *Journal of University of Anbar for Pure Science.* 17(2), 26–35. DOI: 10.37652/juaps.2023.141818.1100.

Alansary, I.M.M., Al-Saryi, N.A., 2022. Detection of biofilm formation in classical and hypervirulent *Klebsiella pneumoniae*. *Al-Mustansiriyah Journal of Science.* 33(5), 65–71. DOI: 10.23851/mjs.v33i5.1315.

Albarri, O., Almatar, M., Öcal, M.M., et al., 2022. Overexpression of efflux pumps AcrAB and OqxAB contributes to ciprofloxacin resistance in clinical isolates of *K. pneumoniae*. *Current Protein & Peptide Science.* 23(5), 356–368. DOI: 10.2174/1389203723666220630162920.

Ali, A.Y., Alani, A.A.K., Ahmed, B.O., et al., 2024. Effect of biosynthesized silver nanoparticle size on antibacterial and anti-biofilm activity against pathogenic multi-drug resistant bacteria. *OpenNano.* 20. DOI: 10.1016/j.onano.2024.100213.

Ali, F.S., Authman, S.H., Al Marjani, M.F., 2019. Imipenem resistance and biofilm formation in *Klebsiella pneumoniae* from some hospitals in Baghdad city. *Journal of Pharmaceutical Sciences and Research.* 11(1), 233–238.

Alipoor, R., Ayan, M., Hamblin, M.R., et al., 2022. Hyaluronic acid-based nanomaterials as a new approach to the treatment and prevention of bacterial infections. *Frontiers in Bioengineering and Biotechnology.* 10, 913912. DOI: 10.3389/fbioe.2022.913912.

Aljarrah, R., Aljobory, A.H., 2017. Structural and optical properties of nanocrystalline CdS films prepared by spray pyrolysis. *World Scientific News.* 87, 175–190.

Ashraf, M.V., Khan, S., Misri, S., et al., 2024. High-altitude medicinal plants as promising source of phytochemical antioxidants to combat lifestyle-associated oxidative stress-induced disorders. *Pharmaceuticals.* 17(8), 975. DOI: 10.3390/ph17080975.

Badry, N., Ebnawaled, A.A., Wahman, M., 2024. Cadmium sulfide nanoparticles: Preparation, characterization, and biomedical applications. *SVU-International Journal of Medical Sciences.* 7(1), 842–864. DOI: 10.21608/svuijm.2024.268358.1797.

Bharatham, N., Bhowmik, P., Aoki, M., et al., 2021. Structure and function relationship of OqxB efflux pump from *Klebsiella pneumoniae*. *Nature Communications.* 12(1), 5400. DOI: 10.1038/s41467-021-25679-0.

Bokatyi, A.N., Dubashynskaya, N.V., Skorik, Y.A., 2024. Chemical modification of hyaluronic acid as a strategy for the development of advanced drug delivery systems. *Carbohydrate Polymers.* 337, 122145. DOI: 10.1016/j.carbpol.2024.122145.

Busi, S., Prasad, R. (Eds.), 2024. *ESKAPE Pathogens: Detection, Mechanisms and Treatment Strategies*. Springer Nature.

Chan, B.K.W., Wong, M.H.Y., Chan, E.W.C., et al., 2022. Transcriptional regulation and functional characterization of the plasmid-borne *oqxAB* genes in *Salmonella typhimurium*. *Microbiology Spectrum.* 10(2), 2170–2191. DOI: 10.1128/spectrum.02170-21.

Curcio, M., Vittorio, O., Bell, J.L., et al., 2022. Hyaluronic acid within self-assembling nanoparticles: Endless possibilities for targeted cancer therapy. *Nanomaterials.* 12(16). DOI: 10.3390/nano12162851.

Dabhane, H., Ghotekar, S., Tambade, P., et al., 2021. A review on environmentally benevolent synthesis of CdS nanoparticle and their applications. *Environmental Chemistry and Ecotoxicology.* 3, 209–219. DOI: 10.1016/j.enceco.2021.06.002.

Dalei, K., 2014. *Synthesis and characterization of cadmium sulphide nanoparticles and its utilization in removal of cadmium from aqueous solution*. Doctoral dissertation.

Dubey, P.R., Kaur, G., Shukla, R., 2025. Nano-mediated management of metal toxicity-induced neurodegeneration: A critical review. *Molecular Neurobiology.* 62, 8400–8419. DOI: 10.1007/s12035-025-04782-z.

Ebrahim, F., Al-Hartomy, O., Wageh, S., 2023. Cadmium-based quantum dots alloyed structures: Synthesis, properties, and applications. *Materials.* 16(17). DOI: 10.3390/ma16175877.

El-Hamid, M.I., Ibrahim, D., Abdelfattah-Hassan, A., et al., 2024. Silver nanoparticles loaded with pomegranate peel extract and hyaluronic acid mediate recovery of cutaneous wounds infected with *Candida albicans*. *Frontiers in Cellular and Infection Microbiology.* 14. DOI: 10.3389/fcimb.2024.1469493.

Elashkar, E., Alfaraj, R., El-Borady, O.M., et al., 2025. Novel silver nanoparticle-based biomaterials for combating *Klebsiella pneumoniae* biofilms. *Frontiers in Microbiology.* 15. DOI: 10.3389/fmicb.2024.1507274.

Fils, P.E., Cholley, P., Gbaguidi-Haore, H., et al., 2021. ESBL-producing *Klebsiella pneumoniae* in a university hospital: Molecular features, diffusion of epidemic clones and evaluation of cross-transmission. *PLoS One.* 16(3). DOI: 10.1371/journal.pone.0247875.

Gaurav, A., Bakht, P., Saini, M., et al., 2023. Role of bacterial efflux pumps in antibiotic resistance, virulence, and strategies to discover novel efflux pump inhibitors. *Microbiology.* 169(5). DOI: 10.1099/mic.0.001333.

Guo, Y., Song, G., Sun, M., et al., 2020. Prevalence and therapies of antibiotic resistance in *Staphylococcus aureus*. Frontiers Media S.A. 10, 107. DOI: 10.3389/fcimb.2020.00107.

Hajiagha, M.N., Kafil, H.S., 2023. Efflux pumps and microbial biofilm formation. *Infection, Genetics and Evolution.* 112, 105459. DOI: 10.1016/j.meegid.2023.105459.

Hamid, L.L., El-Subeyhi, M., Hamed, H., et al., 2024. Preparation and characterization of polyethylene glycol/sodium alginate aerogel beads loaded with biogenic zinc oxide nanoparticles: Potential therapeutic option for treating multidrug-resistant bacteria and cytotoxic activity. *Polymer Bulletin.* 81(18), 16999–17016. DOI: 10.1007/s00289-024-05505-5.

Hetta, H.F., Ramadan, Y.N., Al-Harbi, A.I., et al., 2023. Nanotechnology as a promising approach to combat multidrug-resistant bacteria: A comprehensive review and future perspectives. *Biomedicines.* 11(2). DOI: 10.3390/biomedicines11020413.

Hovhannisyan, A., Janik, M., Woszczak, L., et al., 2023. The preparation of silver and gold nanoparticles in hyaluronic acid and the influence of low-pressure plasma treatment on their physicochemical and microbiological properties. *International Journal of Molecular Sciences.* 24(24). DOI: 10.3390/ijms242417285.

Huang, L., Wu, C., Gao, H., et al., 2022. Bacterial multidrug efflux pumps at the frontline of antimicrobial resistance: An overview. *Antibiotics.* 11(4). DOI: 10.3390/antibiotics11040520.

Jang, S., 2023. AcrAB-TolC, a major efflux pump in Gram-negative bacteria: Toward understanding its operation mechanism. *BMB Reports.* 56(6), 326–334. DOI: 10.5483/BMBRep.2023-0070.

Jassim, S.A., Hassan, M.H., 2023. Neem leaf extract as a potential antibiofilm and anti-ESBLs agent for *K. pneumoniae*. *Research Journal of Pharmacy and Technology.* 16(1), 159–162. DOI: 10.52711/0974-360x.2023.00029.

Kaliyaperumal, R., Nagaraj, K., Kasilingam, T., et al., 2025. Characterization and multifunctional bioactivity of cadmium oxide-modified graphitic carbon nitride (CdO/G-C3N4) nanocomposites for biomedical applications. *BioNanoScience.* 15(3), 402. DOI: 10.1007/s12668-025-02011-4.

Karami-Zarandi, M., Rahdar, H.A., Esmaeili, H., et al., 2023. *Klebsiella pneumoniae*: An update on antibiotic resistance mechanisms. *Future Microbiology.* 18(1), 65–81. DOI: 10.2217/fmb-2022-0097.

Khaleel, D., Huang, X., Mutter, T., 2025. Abundance of capsule-associated genes among *Klebsiella pneumoniae*and the relationship with biofilm formation. *Journal of University of Anbar for Pure Science.* 19(1), 23–31. DOI: 10.37652/juaps.2024.151564.1285.

Khaleel, D.S., Mutter, T.Y., Hamid, L.L., Hassan, O.M., 2025. Morphological transformation of silver nanoparticles to nanofibers via gallic acid conjugation: A synergistic approach against multidrug-resistant pathogens. *Chemical Engineering Journal Advances.* 19, 100836. DOI: 10.1016/j.ceja.2025.100836.

Khaleel, D.S., Mutter, T.Y., Huang, X., 2024. Potential mechanism of gallic acid-coated iron oxide nanoparticles against associated genes of *Klebsiella pneumoniae* capsule, antibacterial and antibiofilm. *Microscopy Research and Technique.* 87(11), 2774–2784. DOI: 10.1002/jemt.24650.

Kim, H., Park, J.H., Choi, Y.J., et al., 2023. Hyaluronic acid-coated gold nanoparticles as a controlled drug delivery system for poorly water-soluble drugs. *RSC Advances.* 13(8), 5529–5537. DOI: 10.1039/D2RA07276A.

Kushwaha, P., Chauhan, P., 2021. Synthesis of spherical and rod-like EDTA-assisted α-Fe2O3 nanoparticles via co-precipitation method. *Materials Today: Proceedings.* 44, 3086–3090. DOI: 10.1016/j.matpr.2021.02.450.

Le, H.V., Le Cerf, D., 2022. Colloidal polyelectrolyte complexes from hyaluronic acid: Preparation and biomedical applications. *Small.* 18(51), 2204283. DOI: 10.1002/smll.202204283.

Lewis II, J.S., 2024. *Performance Standards for Antimicrobial Susceptibility Testing*. Clinical and Laboratory Standards Institute.

Li, G., Li, J., Lee, Y., et al., 2024. Pickering emulsions stabilized by chitosan–flaxseed gum–hyaluronic acid nanoparticles for controlled topical release of ferulic acid. *International Journal of Biological Macromolecules.* 255, 128086. DOI: 10.1016/j.ijbiomac.2023.128086.

Li, J., Zhang, H., Ning, J., et al., 2019. The nature and epidemiology of OqxAB, a multidrug efflux pump. *Antimicrobial Resistance & Infection Control.* 8(1). DOI: 10.1186/s13756-019-0489-3.

Liu, L., Bai, B., Yang, X., et al., 2023. Anisotropic heavy-metal-free semiconductor nanocrystals: Synthesis, properties, and applications. *Chemical Reviews.* 123(7), 3625–3692. DOI: 10.1021/acs.chemrev.2c00688.

Liu, X., Yao, J., Luo, J., et al., 2017. Effect of growth temperature on tailoring the size and aspect ratio of gold nanorods. *Langmuir.* 33(30), 7479–7485. DOI: 10.1021/acs.langmuir.7b01635.

Liu, Z., Lin, W., Liu, Y., 2022. Macrocyclic supramolecular assemblies based on hyaluronic acid and their biological applications. *Accounts of Chemical Research.* 55(23), 3417–3429. DOI: 10.1021/acs.accounts.2c00462.

Mohanty, H., Pachpute, S., Yadav, R.P., 2021. Mechanism of drug resistance in bacteria: Efflux pump modulation for designing of new antibiotic enhancers. *Folia Microbiologica.* 66(5), 727–739. DOI: 10.1007/s12223-021-00910-z.

Nag, A., Mehra, S., 2021. A major facilitator superfamily (MFS) efflux pump, SCO4121, from *Streptomyces coelicolor* with roles in multidrug resistance and oxidative stress tolerance and its regulation by a MarR regulator. *Applied and Environmental Microbiology.* 87(7), 2238–2258. DOI: 10.1128/AEM.02238-20.

Nasrin, T., Patra, M., Escudey, M., et al., 2019. Biosynthesized CdS nanoparticles disturb *E. coli* growth through reactive oxygen production. *Microbial Pathogenesis.* 135, 103639. DOI: 10.1016/j.micpath.2019.103639.

Obaid, W.F., Hasson, S.O., 2021. Pattern of multi drug resistance with biofilm formation among *Klebsiella pneumoniae* isolated from fecal samples of diarrheal Iraqi patients. *Annals of the Romanian Society for Cell Biology.* 25(3), 5350–5360.

Pedroso-Santana, S., Fleitas-Salazar, N., 2023. The use of capping agents in the stabilization and functionalization of metallic nanoparticles for biomedical applications. *Particle & Particle Systems Characterization.* 40(2), 2200146. DOI: 10.1002/ppsc.202200146.

Rather, A.H., Wani, T.U., Khan, R.S., et al., 2022. Recent progress in the green fabrication of cadmium sulfide and cadmium oxide nanoparticles: Synthesis, antimicrobial and cytotoxic studies. *Materials Science and Engineering: B.* 286. DOI: 10.1016/j.mseb.2022.116022.

Raval, H., Bhattacharya, S., 2025. Exploring the potentials of hyaluronic acid-coated polymeric nanoparticles in enhanced cancer treatment by precision drug delivery, tackling drug resistance, and reshaping the tumour microenvironment. *Current Medicinal Chemistry.* 32(20), 3960–3999. DOI: 10.2174/0109298673302510240328050115.

Regassa, B.T., Tosisa, W., Eshetu, D., et al., 2024. Correction: Antimicrobial resistance profiles of bacterial isolates from clinical specimens referred to Ethiopian Public Health Institute: Analysis of 5-year data. *BMC Infectious Diseases.* 24. DOI: 10.1186/s12879-023-08921-6.

Ren, J., Wang, M., Zhou, W., et al., 2024. Efflux pumps as potential targets for biofilm inhibition. *Frontiers in Microbiology.* 15, 1315238. DOI: 10.3389/fmicb.2024.1315238.

Sharma, S., Mohler, J., Mahajan, S.D., et al., 2023. Microbial biofilm: A review on formation, infection, antibiotic resistance, control measures, and innovative treatment. *Microorganisms.* 11(6). DOI: 10.3390/microorganisms11061614.

Spitzmüller, L., Nitschke, F., Rudolph, B., et al., 2023. Dissolution control and stability improvement of silica nanoparticles in aqueous media. *Journal of Nanoparticle Research.* 25(3), 40. DOI: 10.1007/s11051-023-05688-4.

Xu, Q., Jiang, J., Zhu, Z., et al., 2019. Efflux pumps AcrAB and OqxAB contribute to nitrofurantoin resistance in a uropathogenic *Klebsiella pneumoniae* isolate. *International Journal of Antimicrobial Agents.* 54(2), 223–227. DOI: 10.1016/j.ijantimicag.2019.06.004.

Yaaqoub, Z., Abbas, N.K., 2023. Green synthesis of CdS:Sn NPs by starch as a covering agent and studying its physical properties. *Baghdad Science Journal.* 20(5). DOI: 10.21123/bsj.2023.7290.

Yahyaei, B., 2016. Production, assessment, and impregnation of hyaluronic acid with silver nanoparticles produced by *Streptococcus pyogenes* for tissue engineering applications. *Applied Biological Chemistry.* 59(2), 227–237. DOI: 10.1007/s13765-016-0147-x.

Zamboni, F., Wong, C.K., Collins, M.N., 2022. Hyaluronic acid association with bacterial, fungal and viral infections: Can hyaluronic acid be used as an antimicrobial polymer for biomedical and pharmaceutical applications? *Bioactive Materials.* 19(2), 485. DOI: 10.1016/j.bioactmat.2022.04.023.

Zayerzadeh, E., Koohi, M.K., 2024. Application of nanotechnology in novel nano-based compounds development for metal poisoning treatment. *Nanomedicine Research Journal.* 9(2), 120–130. DOI: 10.22034/nmrj.2024.02.002.